Étude détaillée du brouillard à l'aide d'un modèle colonne

Les chapitres précédents nous ont permis de décrire le modèle utilisé ainsi que les données disponibles pour notre étude sur le brouillard. On présente ci-dessous une simulation détaillée (comparaisons aux observations) avec une version 1D de Code_Saturne (modèle colonne) et une analyse de sensibilité afin de connaître l'influence du choix de nos paramétrisations sur l'évolution du brouillard.

Sommaire

3.1 Introduction

Pourquoi réaliser des simulations 1D alors que de nombreuses études ont déjà été menées dans ce domaine ? On peut apporter les réponses suivantes : Le cadre 1D, de par sa simplicité de mise en oeuvre, permet de tester, dans des conditions simplifiées mais réalistes, la plupart des paramétrisations physiques nécessaires à décrire l'évolution du brouillard et des nuages bas. Nous avons cherché à être au niveau de l'état de l'art dans le domaine de complexité que nous avons choisi à savoir : un schéma semi-spectral des nuages chauds. Les analyses de sensibilité, qui ont été menées sur une situation bien documentée, vont nous permettre de déterminer les facteurs les plus importants. C'est une première étape indispensable avant d'appréhender les processus plus complexes de la dynamique en 3D sur un site comme le SIRTA.

Lors des travaux de Bouzereau et al. (2007), une paramétrisation semi-spectrale des nuages chauds a été développée afin de simuler les panaches d'aéroréfrigérants des centres de production thermiques d'EDF. Nous proposons de la valider sur les données de la campagne ParisFog. Dans un premier temps, il nous a semblé souhaitable de tester l'ensemble des paramétrisations physiques (turbulence, rayonnement, microphysique, interface sol-atmosphère) et de leurs interactions sur des cas bien documentés en utilisant une version 1D de *Code_Saturne* ***Atmo***, que l'on appelle *modèle colonne* (voir Fig. 3.1).

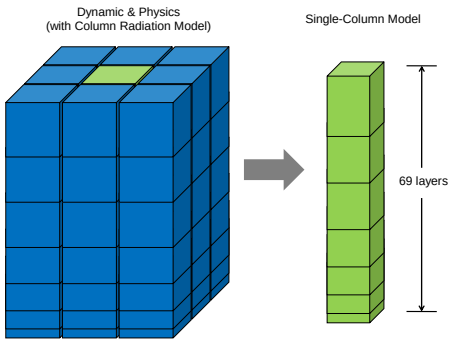

Fig. 3.1 : *Schéma d'un modèle colonne*

Ce modèle colonne calcule l'évolution temporelle des différentes variables météorologiques en différents point d'un maillage *3D* couvrant l'ensemble de la couche limite atmosphérique. Le maillage est constitué dans le plan horizontal de 9 cellules (3×3), mais seules les grandeurs météorologiques dans la cellule centrale sont considérées. Les cellules de bord sont placées suffisamment loin de la cellule centrale pour éliminer l'influence de la diffusion horizontale et l'advection est débranchée. La colonne verticale comprend 69 niveaux, avec le premier niveau (cellule centrée) à 2 m et la dernière à 2672 m. Cependant, les calculs radiatifs sont réalisés sur toute la colonne atmosphérique jusqu'à 11 km.

Dans la partie de l'atmosphère hors du domaine de calcul (supérieur au dernier niveau du maillage), on prend des profils issus du modèle de méso-échelle MM5 ou des radiosondages pour les différentes variables intervenant dans les calculs radiatifs, ainsi que pour diagnostiquer les précipitations lorsque cela est nécessaire.

Afin de s'affranchir de la bonne prévision des conditions synoptiques, le modèle est forcé en se couplant aux radiosondages mesurés sur site par une technique de "nudging". Cela a permis de réaliser des tests de sensibilité aux différents processus microphysiques (nucléation, sédimentation, interaction microphysique nuages-aérosols-rayonnement, ...) dans des conditions réalistes, bien documentées, pour quelques Périodes d'Observations Intensives (POI) durant ParisFog.

La première partie de ce travail est essentiellement constituée de l'article soumis au *Journal of Applied Meteorology and Climatology* : Zhang X., Musson-Genon L., Carissimo B., and Dupont E.. (2009). Numerical sensitivity analysis of a radiation fog event with a single-column model. Submitted to *J. Appl. Meteor. Climatol., in revision.* Elle présente nos résultats sur un cycle de 24 heures démarrant à 12 heures pour la POI-13.

Une deuxième partie porte sur l'étude de l'épaisseur du brouillard pour des simulations démarrant à 21 TU, plus proche de l'heure de formation du brouillard (2230 TU).

3.2 Numerical sensitivity analysis of a radiation fog event with a single-column model

Abstract

This paper presents a detailed numerical simulation of a radiation fog event with a state-of-the-art model. The study includes sensitivity analysis and model validation with observational data from the ParisFog campaign, which took place in the south of Paris during winter 2006-2007. The database is divided into two parts. The first part is constituted by assimilating the maximum of data collected (temperature, humidity, and wind velocity) as possible, which is used to investigate the relative importance among turbulence, radiation, and microphysics for radiation fog simulation. The remaining data (LWC, visibility, and cloud droplet size spectrum) make the second part, which is used for model validation. The validation technique applied is to compare the simulated results using one-dimensional version of the 3D computational fluid dynamical model *Mercure_Saturne* to one of the best collected in situ data during the ParisFog campaign. Special attention is given to the detailed and complete simulations. Several parameterizations for turbulence, nucleation and sedimentation have been described. The present results will be subsequently used for a statistical study of radiation fog events in forecasting mode over a long period.

The comparison between the simulated and the observed visibility, in the single-column model case-study, shows that the evolution of radiation fog is correctly simulated. The analysis of the behavior of the different parameterized physical processes suggests that

the subtle balance between the various processes is nearly achieved. This study also reveals that the fog evolution strongly depends on the turbulent exchange coefficients, the condition of cloud droplet activation, and the sedimentation velocity.

3.2.1 Introduction

Fog is an important meteorological phenomenon, which can have serious negative impacts on air quality, airport operations, and highway safety. Radiative cooling and horizontal movement (advection) are the two main physical processes responsible for fog formation. Fog can be classified as radiative when the first mechanism dominates and as advective when the second is prominent. A radiation fog event is a result of the complex interaction between the land surface and the lower layers of the atmosphere. Its development is primarily controlled by a balance between radiative cooling and turbulence. Meanwhile, the role of cloud microphysics also emerges as important factor.

In recent years, there has been impressive progress in fog simulation and prediction. In statistical model, a highly valued and innovative scientific research was carried out by using artificial neural network techniques in the field of fog forecasting (Fabbian et al., 2007) ; In ensemble forecast and assimilation system, single-column model (hereafter noted as SCM) with high vertical-resolution and variational approach were used to provide accurate forecasting of fog events (Bergot et al., 2005; Müller et al., 2007; Roquelaure and Bergot, 2008) ; In detailed numerical simulation, Nakanishi (2000) has studied the 3D structure of radiation fog, focusing on the dynamic and generation mechanism with Large-Eddy Simulation (LES). On the other hand, from a climatological point of view, Westcott (2007) has developed a fog climatology to examine the surface weather conditions at dense fog onset and during dense fog events for the period 1948-1996. Nevertheless, even if SCMs are extensively used, a benchmark of such models gives the important scattering result concerning the occurrence and dissipation time of fog (Bergot et al., 2007). It is generally accepted that various observations and measurements with a high spatial resolution are fundamental for fog forecasting, such as the Fog-82 campaign in Albany, NY USA (Meyer et al., 1986), Cabauw in Netherlands (Musson-Genon, 1987; Duynkerke, 1991; Nakanishi, 2000), Lille in north of France (Guedalia and Bergot, 1994), and Po Valley in Northern Italy (Fuzzi et al., 1992, 1998). Further, if lack of detailed observations, the fluid-mechanical instabilities occurring in the fog layer cannot be investigated satisfactorily (Nakanishi, 2000). So, a more detailed and complete experimental work is required. As an original contribution, a 6-month cooperative field experiment, named ParisFog was conducted at the SIRTA Observatory (20km South Paris), France, from November 2006 to March 2007, to monitor simultaneously all physical processes (dynamical and microphysical) that drive formation and dissipation of radiation fog (Haeffelin et al., submitted).

Today, in order to improve the physical parameterization schemes and better understand the relevant physical processes of radiation fog, the development of new fog models as well as the improvement of existing models could lead to the goal. In this paper, we

purpose a SCM and assess its ability to reproduce the main mechanisms of fog formation and dissipation, in particular liquid water evolution, horizontal visibility evolution and cloud droplet size spectrum. A case study is chosen from the ParisFog database to test the SCM against a real event, the Intensive Observation Period (IOP) number 13, which is one of the best documented. Because of the simplicity of running a SCM, we can "inexpensively" perform sensitivity tests, furthermore, when developing and testing a new parameterization it can be useful to keep the large-scale atmospheric circulation fixed so that a better assessment can be made of the impact on the local climate without the complication of large-scale feedback (Randall et al., 1996). We begin by a description of the SCM with particular emphasis on the treatment of cloud droplet microphysics. The modeling approach and sensitivity tests are then analyzed. The paper concludes with a discussion of the results and perspectives for the comparison on a long series of fog events.

3.2.2 ParisFog field experiment

The observations used in this study are routine measurements collected at the SIRTA observatory (48.713°N and 2.208°E), which is located 20 km south of Paris, on the campus of Ecole Polytechnique in Palaiseau. The SIRTA site can be considered as a semi-urban environment divided equally in agricultural fields, wooded areas, and housing and industrial developments. The objective of the ParisFog field campaign was to document the radiative, thermodynamical and dynamical processes during the fog life cycle. This program produced a large dataset which has become the focal point of analysis and fog research. A comprehensive classification of the 36 fog and near-fog events sampled during the ParisFog shows the large variability of observed situations with predominant occurrences of radiation fog and stratus cloud. It demonstrates the processes involved in fog formation and development, including the role of radiation, microphysics, turbulence, and moisture transport over heterogeneous terrain. The full details of the ParisFog field project and the instruments used to collect data can be found in Bergot et al. (2008).

3.2.3 Model description

The atmospheric SCM used in this study is the one-dimensional version of the computational fluid dynamics model *Mercure_Saturne*, which is the 3D model adapted to atmospheric flow and pollutant dispersion, developed at CEREA (joint laboratory École Nationale des Ponts et Chaussées-EDF R&D, Université Paris Est). *Mercure_Saturne* model has been tested and validated for the numerical simulation of cooling tower plume (which can be considered as an artificial cloud) by Bouzereau et al. (2008). A detailed description of the warm cloud microphysical scheme can be found in Bouzereau et al. (2008), so only a brief summary and some recent improvements will be given here.

Mercure_Saturne solves the basic set of classical time averaging (Reynolds averaging) and density weighted time averaging (Favre averaging) equations that include classical Navier-Stokes, species, and energy transport equations. The SCM represents an isolated column of atmosphere extending upwards from, and including, the underlying surface.

The model can be forced every time step by advection obtained from observational data or operational analysis or being nudged toward "observed" background. The model is integrated in a 69-level vertical grid, with the lowest level at about 2-meter above the ground and the highest at 2500 m. The main characteristics of the physical package related to warm-cloud modeling in the *Mercure_Saturne* are described below.

Microphysics

In *Mercure_Saturne*, the thermodynamic equations are derived from the conservation of moist static energy (Betts, 1973). The variables chosen are conservative during condensation process. They are given by :

$$\theta_l = \theta - \frac{L_v \theta}{C_p T} q_l, \;\; q_w = q + q_l, \tag{3.1}$$

where θ_l is the liquid potential temperature, θ is the potential temperature, L_v is the latent heat of vaporization, C_p is the heat capacity at constant pressure, T is the temperature in Kelvin, q_w is the sum of water vapor q and LWC q_l. Here, q_l is diagnosed from the predicted value of q by using a subgrid condensation scheme including supersaturation effect.

Additionally, for many cloud modeling purposes, it is necessary to be able to approximate an observed cloud droplet size distribution by an analytical expression. In *Mercure_Saturne*, warm cloud droplets are assumed to follow a lognormal distribution. This distribution function has been employed by Bouzereau et al. (2008) to simulate the cooling tower plume, and will be used in this paper for sensitivity analysis. The number of cloud droplets whose diameter lies in the range r and $r + dr$ is given by :

$$n_c(r) = \frac{N_c}{r\sqrt{2\pi}\ln\sigma_c} \exp\left[-\frac{(\ln r/r_0)^2}{2\ln^2\sigma_c}\right], \tag{3.2}$$

where r is the cloud droplet radius, and $n_c(r)dr$ is the number of cloud droplets in the radius range dr. Also, N_c is the total droplet number concentration per unit volume, σ_c is the standard deviation of the distribution and r_0 is the median radius.

In this way, the warm cloud microphysics can be described by three prognostic variables : the liquid potential temperature θ_l, the total water content q_w, and the cloud droplet number concentration N_c. The corresponding equations take the following form :

$$\rho\left(\frac{\partial}{\partial t} + u_i\frac{\partial}{\partial x_i}\right)\theta_l = \frac{\partial}{\partial x_i}\left[\left(\frac{\lambda_c}{C_p} + \frac{\mu_t}{P_r}\right)\frac{\partial\theta_l}{\partial x_i}\right] - \frac{\theta}{TC_p}\frac{\partial F_{rad}}{\partial z} - \rho\frac{L_v\theta}{C_pT}\left(\frac{\partial q_l}{\partial t}\right)_{\text{SED}}, \tag{3.3}$$

$$\rho\left(\frac{\partial}{\partial t} + u_i\frac{\partial}{\partial x_i}\right)q_w = \frac{\partial}{\partial x_i}\left[\left(\frac{\lambda_c}{C_p} + \frac{\mu_t}{P_r}\right)\frac{\partial q_w}{\partial x_i}\right] + \rho\left(\frac{\partial q_l}{\partial t}\right)_{\text{SED}}, \tag{3.4}$$

$$\rho\left(\frac{\partial}{\partial t} + u_i\frac{\partial}{\partial x_i}\right)N_c = \frac{\partial}{\partial x_i}\left[\left(\frac{\lambda_c}{C_p} + \frac{\mu_t}{P_r}\right)\frac{\partial N_c}{\partial x_i}\right] + \rho\left(\frac{\partial N_c}{\partial t}\right)_{\text{C/E}} + \rho\left(\frac{\partial N_c}{\partial t}\right)_{\text{NUC}} + \rho\left(\frac{\partial N_c}{\partial t}\right)_{\text{SCC}} + \rho\left(\frac{\partial N_c}{\partial t}\right)_{\text{SED}}, \tag{3.5}$$

where ρ is the air density, u_i the wind components, λ_c the thermal diffusivity, μ_t the turbulent viscosity, P_r the turbulent Prandtl number and F_{rad} the vertical divergence of net radiative fluxes. The subscript SED refers to the rate of change due to sedimentation ; C/E, condensation/evaporation ; NUC, cloud droplet nucleation ; SCC, self-collection, respectively. In order to close the system (1)-(3), the sink/source terms on the right-hand sides are parameterized in terms of the prognostic variables themselves, as will be explained further below.

Nucleation As we know the radiative characteristics of the clouds (radiative fluxes, divergence, and albedo) are very sensitive to the evolution of their microstructure. For radiation fog, infrared cooling is a main mechanism driving the saturation. In order to take into account this effect, the evolution equation of supersaturation is supplemented with a radiation term. In the following it will be shown that the radiation term in the growth equation of cloud droplets linearly depends on the absorption cross section of a single particle, so that this term becomes more important for the large droplets. In other words, the distribution of the largest droplets is now only limited by their gravitational settling. Therefore, this yields the supersaturation equation including radiative effects :

$$\begin{aligned}\frac{ds_{v,w}}{dt} &= \left(\frac{\zeta L_v g}{R_a C_p T^2} - \frac{g}{R_a T}\right) W - \left(\frac{R_a T}{\zeta e_s} + \frac{\zeta {L_v}^2}{pTC_p}\right)\frac{dq_l}{dt} + \left(\frac{\zeta L_v}{\rho C_p R_a T^2}\right)\frac{\partial F_{rad}}{\partial z} \\ &= A_1 W - A_2 \frac{dq_l}{dt} + A_3 \frac{\partial F_{rad}}{\partial z}, \end{aligned} \tag{3.6}$$

where $s_{v,w}$ is the supersaturation, t is the time, $\zeta = 0.622$ (molecular weight of water/molecular weight of air), g is the gravity, R_a is the gas constant for dry air, W is the updraft velocity, and e_s is the saturation vapor pressure of water.

As the primary source of cloud droplets, cloud droplet nucleation process depends upon many factors including the characteristics of the aerosols, the updraft velocity of the cloud and the radiation of the clouds, all of which contribute to the level of supersaturation and, therefore, to the amount of aerosols that become cloud droplets. A cloud droplet nucleation parameterization based on Abdul-Razzak et al. (1998) and Abdul-Razzak and Ghan (2000) is used in this study. Compared to implicit parameterizations (such as, Pruppacher and Klett (1997) and Cohard et al. (1998)), it combines the treatment of mono- and multi-modal aerosol distribution consisting of few chemical species. Here, we revisit only the basics, keeping in mind that for multimodal aerosol we need to add over all modes of the aerosol size distribution. With the superposition of three lognormal aerosol distributions, as proposed previously, the number of cloud droplets nucleated at the maximum supersaturation s_{max}, is effectively given by :

$$N_c(s_{max}) = \frac{1}{2}\sum_{i=1}^{3} N_{AP_i}\left[1 - \mathrm{erf}\left(\frac{2\ln\left(s_i/s_{max}\right)}{3\sqrt{2}\ln\sigma_{a_i}}\right)\right], \tag{3.7}$$

where N_{AP_i} is the total aerosol number concentration of mode i, s_i is the critical supersaturation of a particle with the diameter r_{AP_i} and the geometric mean diameter of the aerosol

mode i. It can be calculated by using the Köhler theory. The maximum supersaturation s_{max} is given by :

$$s_{max} = \sum_{i=1}^{3} \frac{1}{{s_i}^2} \left[f_i \left(\frac{\varsigma}{\eta_i} \right)^{3/2} + g_i \left(\frac{{s_i}^2}{\eta_i + 3\varsigma} \right)^{3/4} \right]^{-1/2} \tag{3.8}$$

where :

$$f_i = 0.5 \exp\left(2.5 \ln^2 \sigma_i\right), \tag{3.9}$$

$$g_i = 1 + 0.25 \ln \sigma_i, \tag{3.10}$$

$$s_i = \frac{2\left(2A\right)^{3/2}}{3\sqrt{B} r_{AP_i}}, \tag{3.11}$$

$$\varsigma = \frac{2A}{3} \left(\frac{A_1 W + A_3 \partial F_{rad}/\partial z}{A_4} \right)^{1/2}, \tag{3.12}$$

$$\eta_i = \frac{\left[\left(A_1 W + A_3 \partial F_{rad}/\partial z\right)/A_4\right]^{3/2}}{2\pi \rho_w A_2 N_{AP_i}}, \tag{3.13}$$

with : ρ_w is the water material density, A_1, A_2, A_3 are the constants that have been defined in Eq. (4), and A_4, A, B can be found in Abdul-Razzak et al. (1998).

In addition, there are other two nucleation schemes available in our model : Pruppacher and Klett (1997) and Cohard et al. (1998). They will be compared in the sensitivity analysis section.

Sedimentation The important role of cloud droplet sedimentation in the water budget of radiation fog was first revealed in field observations as well as in the numerical study by Roach et al. (1976) and Brown and Roach (1976). They found that when the sedimentation was not included, the water budget and the modeled LWC was unrealistically large. An adequate mathematical description of the sedimentation process, which depends upon cloud droplet settling velocity V_g , is as follows :

$$\left(\frac{\partial N_c}{\partial t} \right)_{\text{SED}} = \frac{\partial}{\partial z} \int_0^{R_c} V_g(r) n_c(r) dr, \tag{3.14}$$

$$\left(\frac{\partial q_l}{\partial t} \right)_{\text{SED}} = \frac{1}{\rho} \frac{\partial}{\partial z} \int_0^{R_c} V_g(r) \frac{4\pi}{3} r^3 n_c(r) dr. \tag{3.15}$$

Assuming that we are only in the presence of cloud droplets ($r < R_c$ and $R_c = 41\mu m$). The presence of droplets with larger radius ($r > R_c$) would require the activation of precipitation module. Most current numerical fog models deal with droplet settling velocity V_g by using LWC or N_c, or both, as described in Table (3.1) (from BR76 to DD88). However, these parameterizations do not allow taking into account the near-surface phenomenon like fog deposition. So we purpose a new parameterization to calculate

Tab. 3.1 : *Parameterization list of droplet settling velocity (V_g in $m\ s^{-1}$ and N_c in cm^{-3})*

Parameterization	Reference	Abbreviation
$V_g = 62.5q_l$	Brown and Roach (1976)	BR76
$V_g = \alpha(q_l N_c^{-1})^{\beta}$	Corradini and Tonna (1980)	CT80
$V_g = 1.9 \times 10^{-2} q_l$	Kunkel (1984)	K84
$V_g = \max(1.9 \times 10^{-2}, 2 \times 62.5q_l)$	Musson-Genon (1987)	LMG87
$V_g = q_l(N_c \times 10^6)^{2/3} \times 10^6$	Duynkerke and Driedonks (1988)	DD88
$V_g = 1.27 \times 10^8 r^2$	Duynkerke (1991)	D91
$V_g = \rho g C_c r^2 (18\eta)^{-1}$, with C_c being a correction factor for small particles	Zhang et al. (2001)	ZGPB01

V_g from Zhang et al. (2001), in which V_g is calculated as a function of particle size and density, as well as meteorological conditions.

The fog deposition process has long been recognized as an important factor in the water balance of ecosystems (Klemm and Wrzesinsky, 2007). This process of removal by vegetation of fine fog droplet is generally a small component of chemical deposition but is also estimated from the droplet concentration. The deposition flux of fog water, F_{dep}, is predicted from the simple inferential model equation of the type :

$$F_{dep} = q_l R_t^{-1} = q_l V_{dep}, \tag{3.16}$$

where V_{dep} is the deposition velocity ($V_{dep} = R_t^{-1}$), and R_t is the total resistance against deposition and computed as a combination (parallel and serial arrangements) of aerodynamic and surface resistances within the first layer (between the ground surface and the first grid level) : $R_t = R_{aero} + R_{surf}$. The aerodynamic and surface resistances are calculated as :

$$R_{aero} = \frac{\ln(z_1/z_0) - \psi_h}{k_{ar} u^*}, \quad R_{surf} = \frac{1}{\varepsilon_0 u^* (E_{im} + E_{in})}, \tag{3.17}$$

where z_1 is the height at which the deposition velocity V_{dep} is evaluated, z_0 is the roughness height, ψ_h is the stability function, k_{ar} is the Von Karman constant, u^* is the friction velocity, $\varepsilon_0 = 3$ is an empirical constant for all type of land, and E_{im}, E_{in} are collection efficiency from impaction and interception, respectively, which were defined in Zhang et al. (2001).

Finally, if a deposition process is taken into account in the model, the new droplet settling velocity will be calculated as the sum of V_g and V_{dep}.

Self-collection For fog case, cloud droplet can be lost through evaporation, sedimentation or through self-collection. SCC is the process in which cloud droplets collide and stick

Tab. 3.2 : *Parameterization list of horizontal visibility (*VIS *in m)*

Parameterization	Reference	Abbreviation
$VIS = 0.027 q_l^{-0.88}$	Kunkel (1984)	K84
$VIS = 80 N_c^{-1.1}$	Meyer et al. (1980)	MJL80
$VIS = 44.989 N_c^{-1.1592}$	Gultepe et al. (2006)	GMB06a
$VIS = 1.002 (q_l N_c)^{-0.6473}$	Gultepe et al. (2006)	GMB06b

together, but do not directly reach the size where they precipitate. In order to determine analytically the expression of cloud droplet collection rate, the approach of Seifert and Beheng (2001) has been followed in parts :

$$\left(\frac{\partial N_c}{\partial t}\right)_{\text{SCC}} = -k_c \rho^2 q_l \exp\left(9\sigma_c^2\right) + \varphi_{au} \rho q_l N_c, \tag{3.18}$$

where $k_c = 9.44 \times 10^9$ m^3 kg^{-2} s^{-1}, φ_{au} is the auto-conversion rate and defined in Berry and Reinhardt (1974).

Visibility As the work of Gultepe et al. (2006) indicate, the visibility should be parameterized as a function of both LWC and N_c. The different parameterizations proposed in the literature are listed here (Table 3.2) and will be tested in the sensitivity analysis section.

Turbulent closure

The parameterization of turbulent fluxes is an extremely important aspect of one-dimensional modeling of the boundary layer. The exchanges due to turbulent transport are universally recognized as the major factors for fog evolution. The lack of turbulence precludes fog growth, but an excess vertical turbulence will give a strong mixing with high layers that counteract the appearance of fog (Musson-Genon, 1987). The different turbulence closures available in one-dimensional *Mercure_Saturne* are presented by decreasing order of complexity in this section. These different closures are based on the diffusion coefficient relating turbulent fluxes to vertical gradients of the different mean variables.

The $k-\varepsilon$ closure The essence of the $k-\varepsilon$ closure method is to diagnose the values of the diffusion coefficient for the momentum $\mathrm{K_m}$ from the predicted values of the turbulence kinetic energy k and its viscous dissipation rate ε, through the relation $\mathrm{K_m} = C_\mu k^2/\varepsilon$. The values of C_μ and the other constants used in the $k-\varepsilon$ closure were taken from Duynkerke (1988). The energy term is written in following form :

$$\frac{\partial(\rho k)}{\partial t} = \underbrace{-\frac{\partial(\rho W k)}{\partial z} + \frac{\partial}{\partial z}\left(\frac{\mathrm{K_m}}{\sigma_k}\rho\frac{\partial(k)}{\partial z}\right)}_{\text{TRANS}} + \underbrace{\mathrm{K_m}\rho\left[\left(\frac{\partial u}{\partial z}\right)^2 + \left(\frac{\partial v}{\partial z}\right)^2\right]}_{\text{SHEAR}} + \underbrace{\frac{\rho g}{\theta_v}\overline{W'\theta_v'}}_{\text{BUOY}} - \rho\varepsilon, \tag{3.19}$$

where the sources of k are transport (TRANS), shear (SHEAR), and buoyancy (BUOY). The buoyancy flux is computed from the turbulent flux of potential temperature. For buoyancy flux treatment, Duynkerke and Driedonks (1987) and Duynkerke (1988) used an "all or nothing" condensation scheme ; Bougeault (1981) used a partial condensation scheme ; here we use a sub-grid condensation scheme as described by Bouzereau et al. (2007).

The dissipation determined by its evolution equation :

$$\frac{\partial(\rho\varepsilon)}{\partial t} + \frac{\partial(\rho W\varepsilon)}{\partial z} - \frac{\partial}{\partial z}\left(\frac{\mathrm{K_m}}{\sigma\varepsilon}\rho\frac{\partial(\varepsilon)}{\partial z}\right) = \frac{\varepsilon}{k}\left(C_{1\varepsilon}\mathrm{P_{RD}} - C_{2\varepsilon}\rho\varepsilon\right), \tag{3.20}$$

in which $C_{1\varepsilon}$ and $C_{2\varepsilon}$ are constants, and $\mathrm{P_{RD}}$ is the local production of k :

$$\mathrm{P_{RD}} = \mathrm{SHEAR} + \max(0, \mathrm{BUOY}). \tag{3.21}$$

The first-order closure parameterizatoin scheme The Louis turbulence closure (hereafter noted as LTC) (Louis, 1979; Musson-Genon, 1995) is very commonly used in the operational weather forecasting models in Météo France and in European Centre for Medium-range Weather Forecasts (ECMWF). In this closure, turbulent exchange coefficients are computed as a function of mixing length and bulk Richardson number : $\mathrm{K_m} = \left|\frac{\partial U}{\partial z}\right| l^2 F_m(R_i)$, $\mathrm{K_h} = \left|\frac{\partial U}{\partial z}\right| l^2 F_h(R_i)$, where U, l, F_m, F_h, R_i , and $\mathrm{K_h}$ are defined in Musson-Genon (1995), which allow to take into account the effect due to water phase changes.

Here, k and ε can be estimated by using the definition of $\mathrm{K_m}$ and $\mathrm{K_h}$ to use a subgrid condensation scheme with this closure.

Radiation

The radiation exchange plays a primary role in the evolution of fog. For radiation fog, the nocturnal infrared cooling is the predominant effect that brings the air temperature below the saturation threshold. During the fog development phase, the infrared cooling at the top of the fog layer leads to the mixing by turbulence inside the fog layer (cold air above warm air). Solar radiation is active during the day both inside the fog layer and at the ground where solar heating is a major process in fog disappearance. In one-dimensional *Mercure_Saturne*, the radiation scheme is designed to treat separately both longwave and shortwave.

The longwave radiation transfer equation is solved by using the emissivity approximation. Gases absorption is computed for water vapor and its dimers, carbon dioxide and ozone. The effect of cloud is described by transmission functions for LWC overlapping gases absorption by means of extinction coefficient $\mathrm{K_{ext}}$ which does not depend on droplet size distribution. The cloud fraction, as determined in our subgrid condensation scheme, is taken into account following Bougeault (1985).

For solar radiation, a two-band model ($0.2 \sim 0.7\mu m$ and $0.7 \sim 4.0\mu m$) inspired from Lacis and Hansen (1974) scheme is used but with substantial improvements. Delta-Eddington approximation with Joseph's correction (Joseph et al., 1976) is used for the two stream method. Aerosol are now treated as cloud droplets but with different optical properties for single scatter albedo (SSA), asymmetry factor (AF) and optical thickness (OT). Clouds are defined by their LWC, cloud fraction and droplet size distribution that permit to determine a prognostic effective radius. For cloud droplet SSA, we can take into account the charge in pollutant (essentially black carbon) following Sandu et al. (2005), in which the cloud droplet SSA is parameterized as a function of the cloud droplet diameter, the BC's volume fraction, the wavelength and the effective refractive index, or more empirical formulation deduced from observation (Fouquart and Bonnel, 1980). For aerosol SSA, a climatological value of 0.84 for continental area is used following Leighton (1980). Eventually, in order to take into account the pollutant mixture, a more precise determination can be used following Tombette et al. (2008), in which the aerosol SSA depends on the aerosol optical thickness (AOT) and the total AOT : $\omega_a = AOT/AOT_{tot}$. From the original method we keep both the adding method but taking into account cloud fraction and the K distribution method for water vapor/liquid overlap.

External data and objective analysis

It should be noted here that geostrophic wind components and horizontal advection are considered as external forcing parameters in SCM and can be estimated using the output of a mesoscale numerical model or from analyses of observed data. In this paper the horizontal advective terms were derived from observations taken during the ParisFog Intensive Observing Periods (IOPs) at the SIRTA site. In order to perform the physical tests of parameterization in analysis mode, a major problem is how to obtain the data required for the SCM. Because of lack of low-level information in the radiosonde, the 30-m mast and sonic anemometer will be added to the vertical information. Therefore, the process of transforming data from observations at irregularly spatio-temporal points into data at regularly arranged points for the simulation has been referred to as objective analysis technique. In this paper, the objective analysis technique used is based on the Cressman scheme (Cressman, 1959).

The Cressman objective analysis scheme assigns to each observation a circular radius of influence R. The first-guess field at each grid point P(x,t) is adjusted by taking into account all the observations which influence P(x,t). The differences between the first-guess field and the observations are calculated, and a distance-weighted average of these difference values is added to the value of the first-guess at P(x,t). Once all grid points have been adjusted, the adjusted field is used as the first guess for another adjustment cycle. Subsequent passes each use a smaller radius of influence. The weights are an exponential function of distance between grid point and observation. An example is shown in Fig. 3.2.

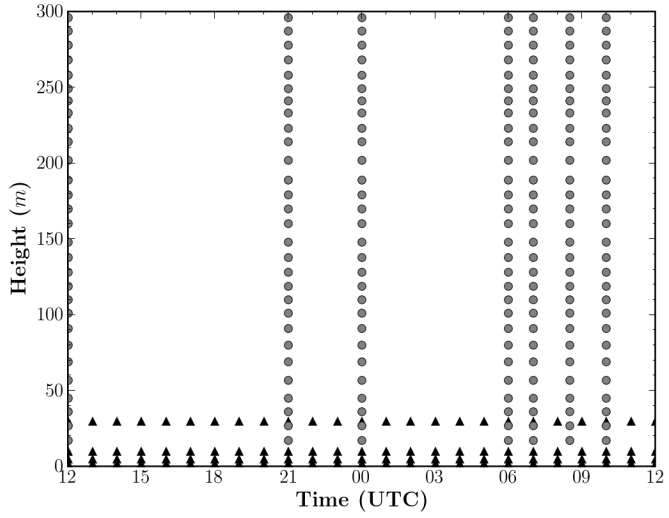

(a)

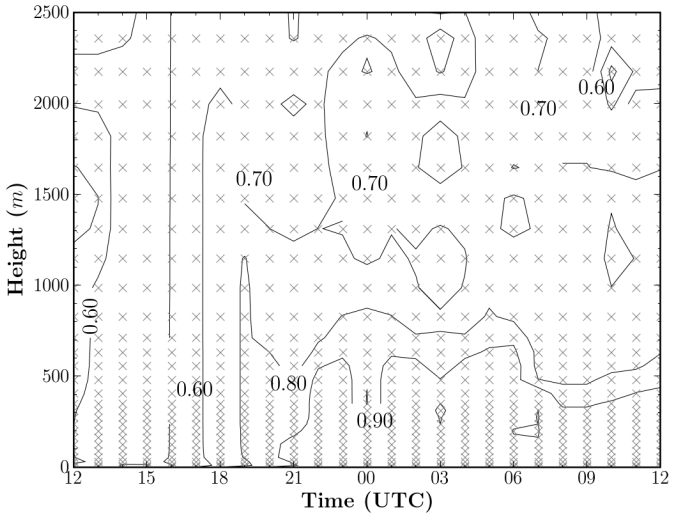

(b)

Fig. 3.2 : *An example of Cressman analysis. (a) spatial-temporal data distribution of the relative humidity over SIRTA site for 18-19 February 2007. Radiosonde data are presented as cirde marker and surface station data are presented as triangle-up marker; (b) interpolation results performed over the mesh grid for the simulation (cross marker present mesh grid).*

Boundary and initial conditions

Boundary conditions need to be physically sound and be specified as accurately as possible. The SCM assumes an atmospheric horizontal-homogeneity and therefore there are only top and bottom boundary conditions to set up. Above the top of the model (2500 m), a symmetry condition is imposed. At the surface (or more precisely at the roughness

height), a rough-wall boundary condition is applied.

The evolutions of land surface temperature T_s and humidity q_s can be treated through two different methods with reasonable results : the force-restore method (FRM) and atmospheric surface layer (ASL) method. The FRM has been employed with considerable success in numerical weather prediction models to estimate diurnal fluctuations in the land surface temperature by using an energy balance equation for the earth's surface (Deardorff, 1978). The ASL method (Musson-Genon et al., 2007), based on the Monin-Obukhov similarity theory, presents a technique for reconstruction of T_s and q_s evolutions based on measurements data of wind, temperature, and humidity at two different levels. This temporal dataset can replace the land-surface atmosphere model and will be imposed at the land surface as external parameters. It can be considered as a land-surface boundary layer forcing condition.

The initial conditions (temperature, humidity and wind) were obtained by Cressman objective analysis scheme from the radiosonde, sonic anemometer and 30-m mast data, as described above.

3.2.4 Simulation

Synoptic background

We will consider the fog that formed on the night of 18-19 February 2007. During the day of 18 February, the northern France is ridged with high pressure ; this brings clear skies and light winds over Palaiseau. As a result, the surface was very effectively cooled by longwave radiation. The temperature at 2-m dropped from 11 °C around sunset (1814 UTC) to a minimum of about 5.0 °C. The downward longwave flux measured showed that there was one short cloud passage during the afternoon, between 1800 and 1900 UTC, before the start of nocturnal cooling. The one-minute average relative humidity increases from about 45% (1300 UTC) to a maximum of nearly 100% during the night. The fog formed on the site toward 2300 UTC and became dense very quickly and this stage was continued until the dissipation (about 0840 UTC). During the fog event, the measurements of droplet number concentration and size distributions are performed, at the 2-m height every 10 minutes, by two PALAS WELAS-2000 particle spectrometers, in the 0.39-40 μm diameter range, with 20% uncertainty on particle number, per size bin.

Control simulation

The control simulation of the event began at 1200 UTC 18 February under the land surface forcing condition and then continued until 1200 UTC February 19 when the fog disappeared completely. Meanwhile, the SCM was operated in "nudging mode", where the temperature, humidity and wind profiles were nudged to the observed analyzed profiles (see above) using a specified time constant τ_n. As Lohmann et al. (1999) indicate, the difficulty is to find a nudging coefficient C_n (inverse of relaxation time : τ_n^{-1} s^{-1}) large enough to force the model close enough toward the observations but small enough to allow

the model to develop its own physical processes. The nudging coefficient used in control simulation was 10^{-4} s^{-1}, which is the same order as the Coriolis parameter. The complete list of the parameterizations used with a brief description of each of the adjustable parameters is shown in Table (3.3). It should be noted that the cloud droplet activation spectrum can be initiated through a fitting procedure by using scanning mobility particle sizer (SMPS) measurements of aerosol number size distribution (Fig. 3.3).

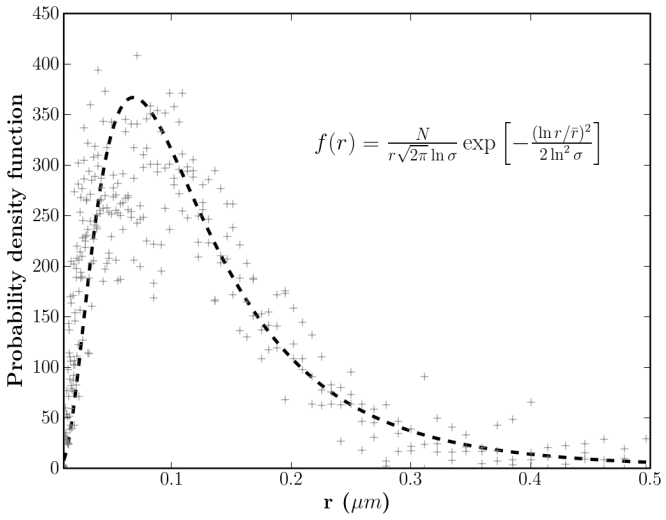

Fig. 3.3 : *Observed aerosol size number distribution (SMPS) with lognormal fits for 1800 UTC 18 February 2007. $N = 550$, $\sigma = 0.69$, and $\bar{r} = 0.11$. SMPS : plus markr, fitted lognormal function : dashed line.*

The surface energy balance is a result of a strong outgoing longwave radiative flux with a small upward ground flux : radiative cooling progresses to the point that the air just above the ground becomes supersaturated and fog droplet begin to form by condensation. After the onset of fog, the situation dramatically changes. The turbulence near the ground grows and the lowest layers of the column mixes up forming the so-called fog layer - the fog development is beginning. The time series of air temperature recorded at different levels, depicted in Fig. 3.4a, clearly shows a typical temperature mixing process and a movement of the inversion to upper levels. Here, we notice a turbulence kinetic energy (hereafter noted as TKE) underestimation of which value is about 30%, especially between 1700 and 0000 UTC (Fig. 3.4b). This TKE underestimation seems to be a common feature of the SCM modeling and this situation might necessitate a 3D modeling, which allows taking explicitly into account the spatial heterogeneity of the environment.

Figs. 3.4c and 3.4d show vertical profiles comparisons between the simulated and the observed (radiosonde data) for temperature and wind intensity, respectively. It should be mentioned that the simulated profiles are correctly reproduced, especially the appearance of a well mixed layer between 0000 and 0003 UTC, increasing within the fog layer. Meanwhile, we also noticed a temperature underestimation at 2100 UTC (Fig. 3.4c), and that is related to the equilibrium between turbulence and radiative cooling before the fog

Tab. 3.3 : *The adjustable parameters studies in the sensitivity experiments. A brief description of the parameter, the control value used and the calculated sensitivities are given.*

Parameterization	Description	Control version	Sensitivity tested
Turbulent closure	Dynamic	$k-\varepsilon$ (Duynkerke, 1988)	Louis (Musson-Genon, 1995)
K_{ext}	Extinction coefficient	120	150
ω_c	Cloud droplet single-scattering albedo	Sandu et al. (2005)	Fouquart and Bonnel (1980)
ω_a	Aerosol single-scattering albedo	Tombette et al. (2008)	Leighton (1980)
NUC	Nucleation term	Abdul-Razzak et al. (1998)	(1) Pruppacher and Klett (1997) ; (2) Cohard et al. (1998)
SED	Sedimentation term	ZGPB01	see Table 3.1
DEPO	Deposition term	ZGPB01	without deposition
SCC	Self-collection term	Seifert and Beheng (2001)	without SCC
C_n	Nudging coefficient	10^{-4}	10^{-3}

appearance. Since the $k - \varepsilon$ closure, the lack of turbulence in the SCM leads to insufficient cooling near the surface, moreover, the longwave radiation scheme ought to be more refined near the surface in order to precisely estimate the infrared cooling. During the

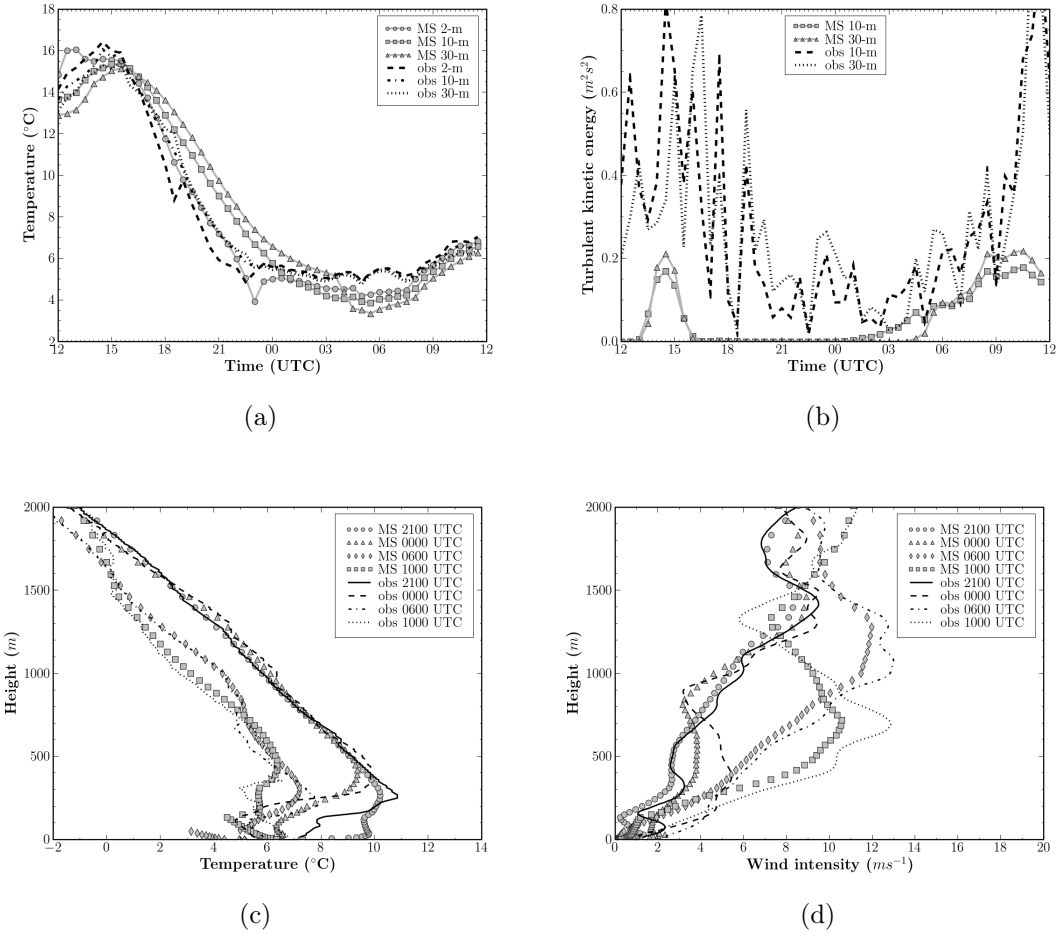

Fig. 3.4 : *Comparison between simulated ("MS") and observed ("obs") for (a) the temperatures at different levels ("2m", "10m", and "30m"), (b) the TKEs at different levels ("10m" and "30m"), (c) the different temperature profiles ("2100 UTC", "0000 UTC", "0600 UTC", and "1000 UTC"), and (d) the wind intensity profiles (with the same legend as (c)).*

initial stage of fog formation, as shown in Fig. 3.5a, infrared cooling continues at near the surface until the fog depth reaches several meters, deep enough to begin to absorb and re-emit radiation originating from the earth. As can be seen in the results reported in the comparison of simulated and observed visibility (Fig. 3.5b), the model correctly predicts the fog formation time with LWC $= 0.05\ g.kg^{-1}$, even though the visibility is about 200 m at this stage that is due to the exceeded temperature by the model at 2100 UTC. The fog dissipation starting at the ground after 0840 UTC is also correctly reproduced. After 0840 UTC the radiative heating near-surface begins to warm the lower portion of the fog layer and the fog begins to dissipate from below.

During the maintenance phase, the fog is more likely contain a large number of small droplets, rather than a small number of large droplets. As shown in Fig. 3.5c, the values and overall size range of droplets simulated are in good agreement with the observation (Fig. 3.5d), especially for the droplet number. However, the width of the cloud droplet spectrum is larger than the observations, this is entirely due to the subgrid condensation scheme used, which systematically exceeded the LWC during the simulation. In addition, we noticed that there are still some small particles present at 0900 UTC (Fig. 3.5d). As mentioned previously, the measurements of droplets has 20% uncertainty on number, this just might make it possible for some large aerosols being sampled.

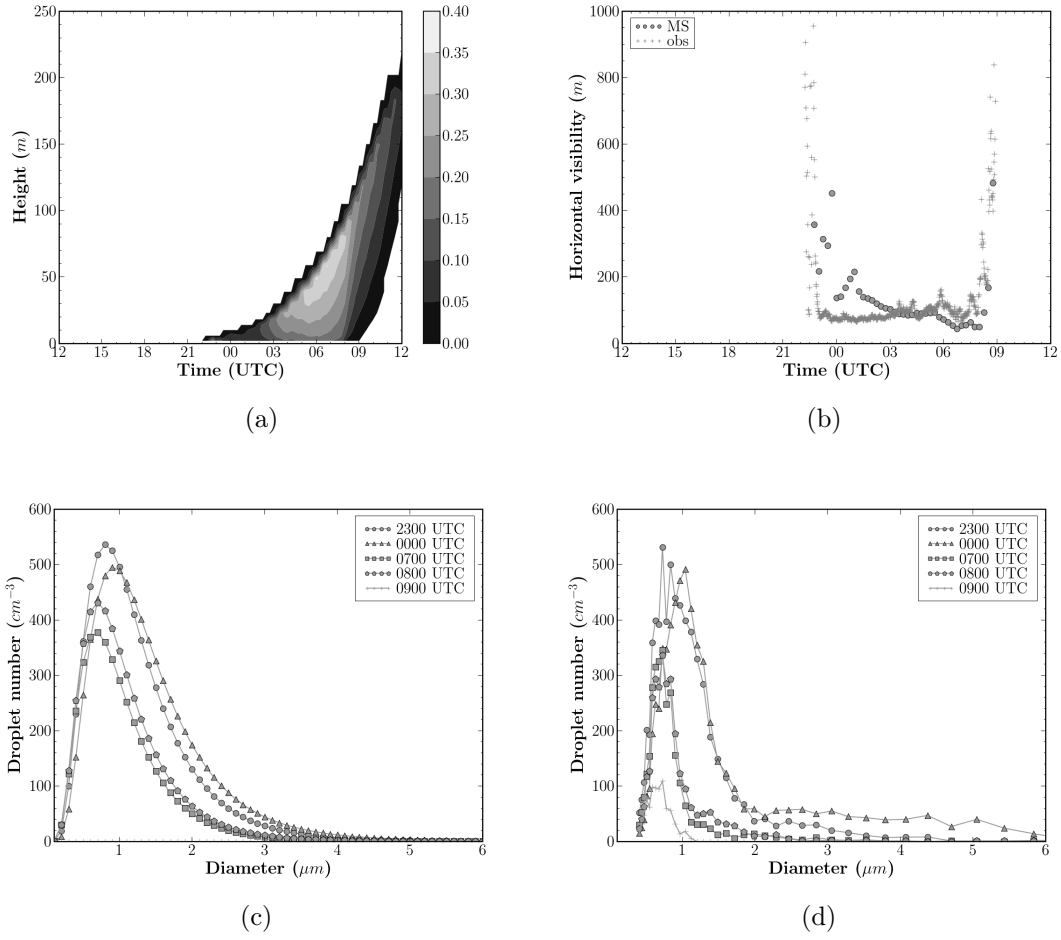

Fig. 3.5 : *Comparison between simulated and observed for (a) the simulated* LWC *time evolution, (b) the horizontal visibility simulated at 2-m height, (c) the cloud droplet size spectrum simulated at 2m height, and (d) the cloud droplet size spectrum observed at 2-m height.*

Here, it is necessary to mention that the value of the logarithmic spread of cloud droplet distribution, σ_c, is an operational variable to be determined. The value used in Bouzereau et al. (2008) was tested firstly and it gave a bias of about 2 μm in the median radius. To adapt for the fog simulation, σ_c is fitted to the observed data of cloud droplets

and this gives an acceptable result. The value will be employed for further work concerning the forecasting of radiation fog.

Sensitivity analysis

In this section, the sensitivity of the model to the various input parameters was tested. The list of the adjustable parameters for the sensitivity tests have been shown in Table (3.3). Besides the aforementioned tests dealing with the physical process, one more influence factor is considered : the treatment of land surface-atmosphere interactions, which plays an important role in predicting fog.

Sensitivity to turbulent closure In these experiments, the simulation was performed with the LTC. In spite of its simplicity, in this case-study, the closure gives comparable results to the $k-\varepsilon$ for near-surface temperature and TKE. However, the results for LWC and horizontal visibility are significantly different from the $k-\varepsilon$. On the whole, this is because the LTC tends to promote greater turbulent entrainment than $k-\varepsilon$. This produces smoother vertical profiles and therefore, the vertical distribution of LWC is different from $k-\varepsilon$ (Fig. 3.6a). On the other hand, the near-surface turbulence attenuates the gradient of temperature and humidity and therefore, the LWC near the surface is less and the fog formation predicted is 1 h late (Fig. 3.6b). However, the fog dissipation is correctly reproduced.

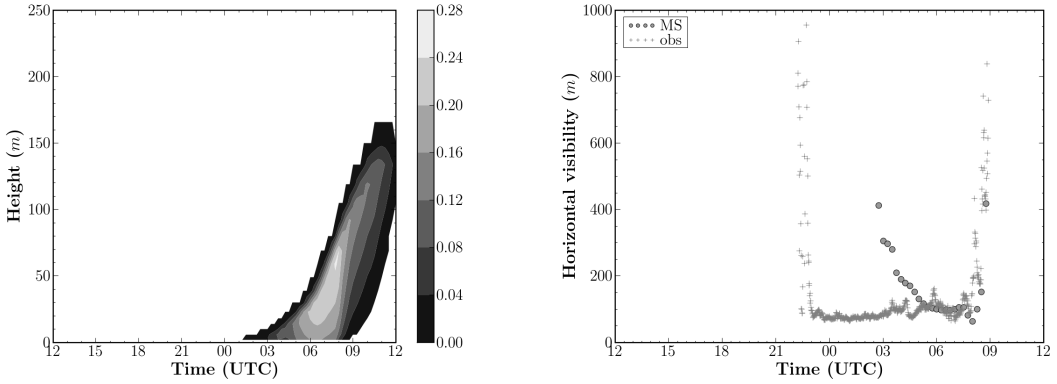

(a) (b)

Fig. 3.6 : *The effects of the Louis closure on (a) the simulated* LWC *time evolution and (b) the horizontal visibility simulated at 2-m height.*

Sensitivity to SSA in the solar radiation In this section we investigate the sensitivity of the model results to the specification of cloud droplet SSA parameterization. Two cloud droplet SSA schemes are examined : (i) Sandu et al. (2005) ; and (ii) Fouquart and Bonnel (1980). The main difference between the two parameterizations is that (i) tends to have greater LWC in the lower atmosphere compared to (ii). This is because the

absorption of solar radiation is partially dependent on the aerosol chemical composition (especially black carbon) incorporated in cloud droplets. The parameterization of Fouquart and Bonnel (1980) seems to exceed the impact of absorption for cloud simulation. However, since the radiation fog usually occurs during night or early morning when solar radiation is absent, the simulation did not make much difference. Nevertheless, to simulate a dense fog event with long duration, it is still necessary to explicitly deduce the droplet SSA from the properties of the background aerosol.

Sensitivity to microphysics

Visibility parameterization test The Fig. 3.7 presents a comparison of different visibility parameterizations proposed by Gultepe et al. (2006), in which the parameterization GMB06a shows good agreement with the observation. Therefore this parameterization will be employed to examine the impacts of sedimentation and nucleation. Since the effects of N_c on the dynamical and thermodynamical variables are very slight, the consideration should be put on the visibility evolution and the water content evolution in following sections.

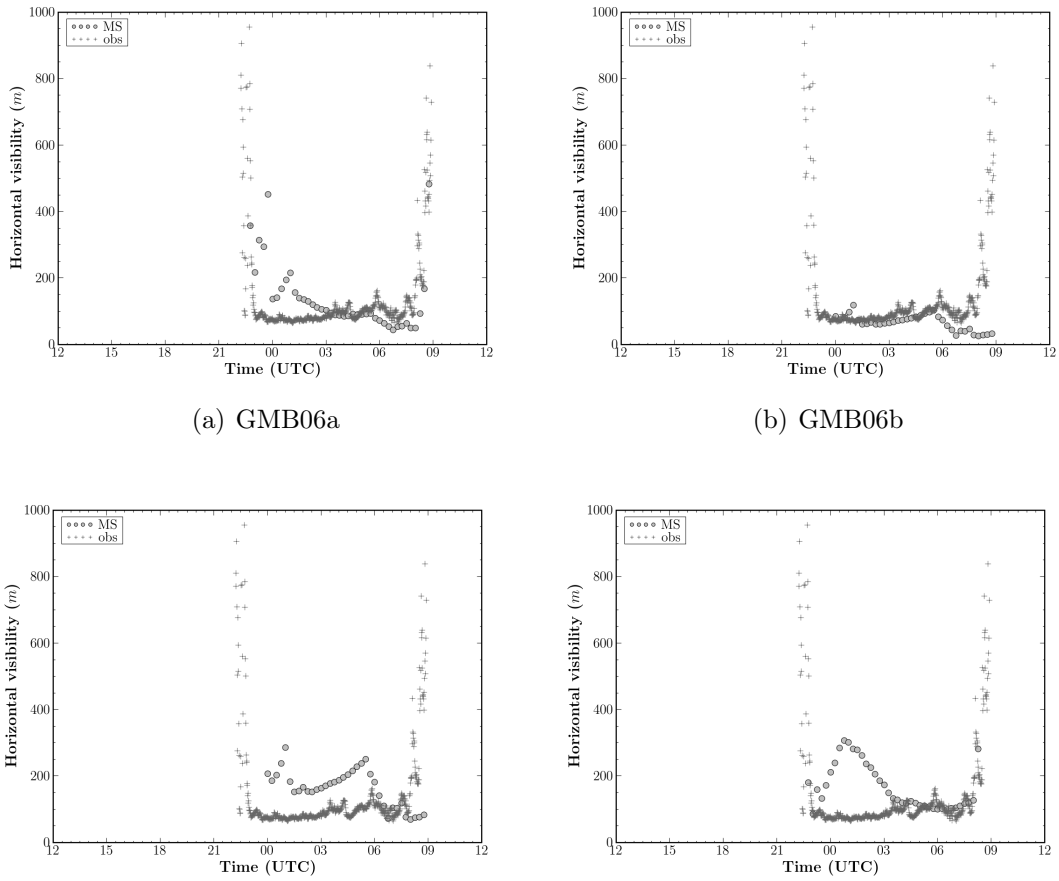

(a) GMB06a (b) GMB06b

(c) MJL80 (d) K84

Fig. 3.7 : *Comparison among different visibility parameterizations (Table 3.2).*

Effect of sedimentation parameterization The parameterization of the sedimentation used in the control run was replaced with alternate schemes in six additional runs (see Table 2.2). These runs produced different LWC and N_c, leading to a large difference in horizontal visibility. In particular, the use of the formula DD88 gives much more LWC in fog mature phase and consequently a delay in fog dissipation (Fig. 3.8a). Moreover, sedimentation of cloud droplets is important as a transport mechanism of liquid water for low levels. The N_c is therefore predicted unrealistically large (Fig. 3.8b). Furthermore, it is necessary to point out that the total suppression of sedimentation term gives an unrealistic LWC, greater than 0.5 $g.kg^{-1}$. For these reasons, an accurate sedimentation parameterization is a necessary condition for forecasting of visibility range.

In this experiment, the effect of droplet deposition is not remarkable for fog evolution. From the deposition parameterization, it is possible that turbulent impaction has primary influence on deposition at high friction velocity. We have a friction velocity of the order of 5 $cm.s^{-1}$ simulated during the occurrence of fog, this may help explain why the liquid water and droplet concentration are little change in the fog life. Furthermore, one case does not guarantee that the simulation will be effective and efficient. We may need more cases with different local condition to study the fog deposition fluxes of water and particle.

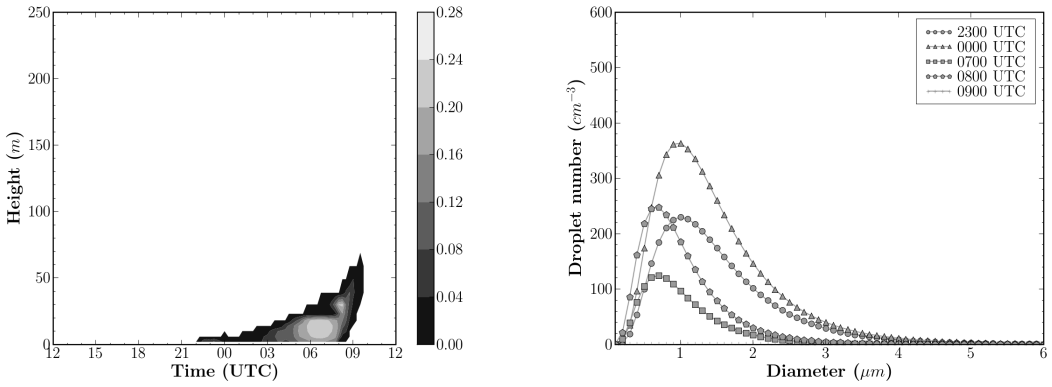

(a) (b)

Fig. 3.8 : *The effects of the sedimentation parameterization of DD88 on (a) the simulated* LWC *time evolution and (b) the cloud droplet size spectrum simulated at 2-m height.*

Effect of nucleation parameterization The same type of test was performed with the other two cloud droplet nucleation parameterizations. It should be noticed that the change of nucleation scheme has only an influence on the cloud droplet number concentration (very slight effect on other variables), as shown in Figs. 3.9a and 3.9b. Since aerosol can act as cloud condensation nuclei, the properties of aerosol in the ambient air play an important role in fog evolution. As a major source, the activation of fog droplet occurs at different supersaturation for different aerosol species. For this reason, the parameterization of Abdul-Razzak et al. (1998) gives good agreement for cloud droplet size spectrum.

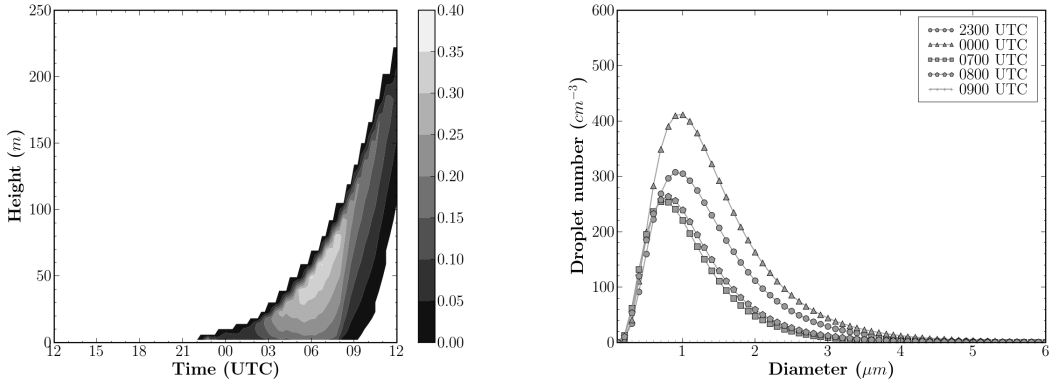

(a) (b)

Fig. 3.9 : *The effects of the nucleation parameterization of Cohard et al. (1998) on (a) the simulated* LWC *time evolution and (b) the cloud droplet size spectrum simulated at 2-m height.*

Simulation with land surface-atmosphere model In this experiment, the temperature at z_0 is computed from the energy balance for the earth's surface (FRM). In the temperature evolution equation, the soil humidity flux will be equal to zero when the air just above the ground is saturated. Fig. 3.10 shows the LWC evolution and the horizontal visibility at 2-m height for this case. The simulation is close to that simulated with forced soil condition. In particular, the model is still able to predict well the fog dissipation phase in the morning. However, the fog evolution predicted, from the formation to the dissipation, is about 1 h late, which indicates that the modeling of the surface energy budget adds an additional uncertainty in operational forecasting models.

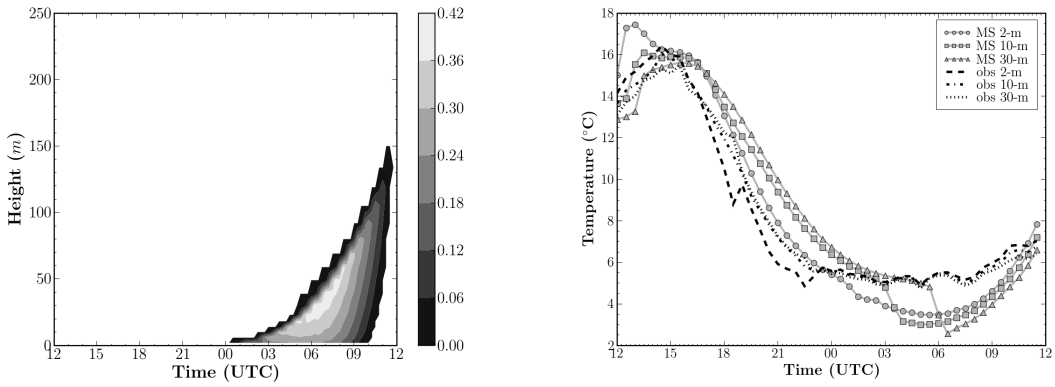

(a) (b)

Fig. 3.10 : *Results performed with land-surface atmosphere model. (a) the simulated* LWC *time evolution ; (b) the temperatures at different levels ("2m", "10m", and "30m").*